# An Experimental Study on Prototype Lithium–Sulfur Cells for Aging Analysis and State-of-Health Estimation

Neda Shateri, Daniel J. Auger, *Senior Member, IEEE*, Abbas Fotouhi, *Member, IEEE*, and James Brighton

***Abstract*— Lithium–sulfur (Li–S) batteries offer potential for higher gravimetric energy density in comparison to lithium–ion batteries. Since they behave quite different from lithium–ion batteries, distinctive approaches to state estimation and battery management are required to be developed specifically for them. This article describes an experimental work to model and perform real-time estimation of the progression of use-induced aging in prototype Li–S cells. To do that, state-of-the-art 19-Ah Li–S pouch cells were subject to cycling tests in order to determine progressive changes in parameters of a nonlinear equivalent-circuit-network (ECN) model due to aging. A state-of-health (SoH) estimation algorithm was then designed to work based on identifying ECN parameters using forgetting-factor recursive least squares (FFRLS). Two techniques, nonlinear curve fitting and support vector machine (SVM) classification, were used to generate SoH values according to the identified parameters. The results demonstrate that Li–S cell's SoH can be estimated with an acceptable level of accuracy of 96.7% using the proposed method under realistic driving conditions. Another important outcome was that the "power fade" in Li–S cells happens at a much slower rate than the "capacity fade" which is a useful feature for applications where consistency of power delivery is important.**

***Index Terms*— Experimental test, lithium–sulfur (Li–S) battery, parameter identification, state-of-health (SoH) estimation, support vector machine (SVM) classifier.**

## I. Introduction

BATTERY technology development is central to vehicle electrification. One near-future technology is lithium–sulfur (Li–S). Compared to existing battery technologies, Li–S may offer potential advantages such as higher specific energy, improved safety, and competitive cost at-scale. However, there are still challenges that limit present-day commercialization such as low power capacities and limited cycle life [1]. Although in recent years, there has been progress in the development of Li–S cells [2], the technology is still not ready for automotive application by considering its requirements [3]. In addition to the researches which are going on by the material scientists and electrochemists to improve each generation of Li–S cells, engineers are also putting effort to make this battery technology ready for market applications. As part of such efforts, this study is focused on the development of a new state-of-health (SoH) estimation technique for Li–S battery to be used in an electric vehicle (EV).

Looking at the literature, novel battery management system (BMS) algorithms are required for Li–S cell chemistry since the existing Li–ion BMS does not work for it [4], [5]. One of these differences is related to the unique shape of Li–S cell's voltage curve that is almost flat in a wide range of battery state-of-charge (SoC). Another difference between Li–ion cells and Li–S is related to the higher rate of self-discharge in Li–S cells. These unique features make Li–S SoC estimation a demanding task as discussed in [6]–[8]. Although Li–S cell SoC estimation has been addressed in a limited number of studies during the last five years, there is still more space to work in that area. In addition to SoC estimation as a main task of a BMS, SoH estimation is also necessary to be performed in real-time applications such as in an EV. Whereas SoC shows the driver how much charge remains in the battery, SoH includes the information about the health of the battery in a quantitative way.

Li–S cell degradation mechanism has been studied quite well in the literature by electrochemists. In [9], electrochemical impedance spectroscopy (EIS) method is used for degradation analysis of Li–S batteries. For this purpose, an equivalent circuit network (ECN) model is used where its elements have been related to physical and chemical processes occurring in the anode, cathode, and electrolyte. In [10], different materials have been investigated to achieve longer life in Li–S cells. A novel strategy has been proposed to develop a highly-stable Li–S cell by building a strongly coupled interface between surface-mediated carbon hosts and various S-containing guests. In another study [11], the impact of different cathode binders on the electrochemical performance of Li–S batteries has been tested and analyzed during cycling. The work presented in [4] gives an insight into understanding of the degradation mechanism in Li–S cells by investigating the surface morphologies and chemical structures of the cathode subject to cycling. Methods such as scanning electron microscopy (SEM), near-edge X-ray absorption fine structure (NEXAFS), and X-ray photoelectron spectroscopy (XPS) have been used in [12].

Although the degradation mechanism in a Li–S cell has been fully studied by electrochemists, there are few studies in the literature where Li–S cell SoH estimation is investigated for BMS application. While electrochemistry-oriented models

Manuscript received November 1, 2020; revised January 13, 2021; accepted February 4, 2021. Date of publication February 16, 2021; date of current version August 24, 2021. This work was supported in part by the European Commission under Grant 814471 and in part by Innovate U.K. under Grant TS/R013780/1. *(Corresponding author: Daniel J. Auger.)*

The authors are with the Advanced Vehicle Engineering Centre, Cranfield University, Cranfield MK43 0AL, U.K. (e-mail: d.j.auger@cranfield.ac.uk).

Digital Object Identifier 10.1109/TTE.2021.3059738

This work is licensed under a Creative Commons Attribution 4.0 License. For more information, see https://creativecommons.org/licenses/by/4.0/

provide valuable insights into degradation mechanisms, they are not suitable for real-time applications because of their high level of computational complexity. In a BMS application, we need quick models/estimators that are able to generate results which are "good enough"—not necessarily accurate enough to describe every electrochemical detail, but sufficient to obtain near-maximum performance and avoid damage and other unwanted events. Two of the studies in the literature, where the Li–S BMS application has been aimed, are presented in [13] and [14]. In those studies, a lab-based test methodology is presented for Li–S cell aging investigation. One of the limitations of those studies is the constant charge/discharge and pulse current profiles, which are applied in the aging experiments instead of realistic profiles. In this study, the cells are subject to a realistic degradation scenario, which is driving cycle tests for EV application. In addition, the Li–S cell that had been used in those previous studies [13], [14] was a small 3.4-Ah Li–S prototype cell, whereas this study investigates a state-of-the-art high capacity (i.e., 19 Ah) Li–S pouch cell. In another study presented in [15], a fresh 3.4-Ah Li–S cell is compared with a similar type aged cell to investigate the effect of aging on cell's capacity and internal resistance. Although the results of that study are promising, they suffer from limited test data. This study aims at filling this research gap by conducting comprehensive aging experiments on state-of-the-art Li–S cells based on some real EV driving cycle scenarios and also designing novel Li–S battery SoH estimators for that application.

The proposed framework in this study is based on Li–S cell ECN model's parameter identification in real-time to be used for cell SoH estimation. For this purpose, different number of identified ECN model's parameters are considered and two methods are used for SoH estimation: 1) first, a nonlinear curve fitting technique is used when only one input parameter is available for SoH estimation and 2) second, combinations of single parameters are considered in a support vector machine (SVM) classifier to estimate SoH. In both cases, recursive least squares (RLS) algorithm is used for cell model identification [16]–[20]. SVM method has been widely used in the literature for modeling, prediction, and classification in different applications since 1998 [21]. SVM technique is particularly used in a variety of engineering subject areas including SoC estimation [22]–[25] and SoH estimation [26]–[32] for Li–ion batteries. In [26] and [27], a method of SoH estimation has been developed using SVM technique by considering both capacity and resistance as the indicators of Li–ion battery degradation for EV application. In [28], relevance vector machine (RVM) technique, that is a Bayesian version of SVM method, has been used for state estimation in combination with the particle filter (PF) method. In [29]–[31], the remaining useful life of a Li–ion cell has been predicted based on SoH estimation using a support vector regression (SVR) model. In another study presented in [32], an optimized combination of features are extracted from terminal voltage response of a Li–ion cell to a short-term current pulse. The features were then used by an SVM model to generate SoH value.

In comparison to the literature, this study has the following contributions.

TABLE I
SPECIFICATIONS OF THE PROTOTYPE LI–S CELL

| Parameter | Value |
|---|---|
| Capacity | 19 (Ah) |
| Nominal voltage | 2.15 (V) |
| Cell mass | 141 (g) |
| Maximum voltage | 2.6 (V) |
| Minimum voltage | 1.9 (V) |
| Maximum discharge rate | 3C ~ 57 (A) |
| Maximum charge rate | 0.25C ~ 4.75 (A) |

1) Experimental degradation test data of a state-of-the-art 19-Ah Li–S pouch cell is presented and analyzed. Real-world driving cycle current profiles are used rather than constant charge–discharge profiles.
2) The effect of aging on Li–S cell ECN model's parameters is investigated as an extension of the previously published works in the literature [6], [40] and a new SoH estimation technique is developed to be used in real-time.

Structure of this article is as follows. In Section II, specifications, characterization test, and the proposed modeling approach of the Li–S cell are explained. Section III then contains the results of Li–S cell degradation tests and SoH estimation using different approaches. The modeling and estimation results of this study are then validated against experimental aging data. In Section IV, a sensitivity analysis is performed and finally, the conclusions are presented in Section V.

## II. LI–S CELL: SPECIFICATIONS, AGING TEST AND MODELING

### A. Li–S Cell Specifications

The Li–S cell that is considered in this study is supplied by OXIS Energy Ltd., U.K. [33] with the specifications listed in Table I. It should be noted that the cell is a prototype with energy density of 290 Wh/kg; however, the final product is expected to have an energy density more than 400 Wh/kg [33].

### B. Li–S Cell Aging-Characterization Test

Fig. 1(a) illustrates the equipment, which are used for cell testing. The test rig consists of a power source/sink, which applies a desirable current profile to the cell and a thermal chamber to keep the temperature at a certain level during the tests. The desired current profile (i.e., a driving cycle scenario here) is programmed using a PC, which communicates with the power source/sink during the tests. The command (i.e., current) is sent to the device at each time step and cell's terminal voltage and the real current signal are measured and sent back to the PC to be recorded. Data are collected in the time domain with a sampling rate of 1 Hz including time, temperature, current, and cell's terminal voltage. All tests are started from fully charged state (2.6 V) and are continued until fully discharged state (based on cutoff voltage of 1.9 V).

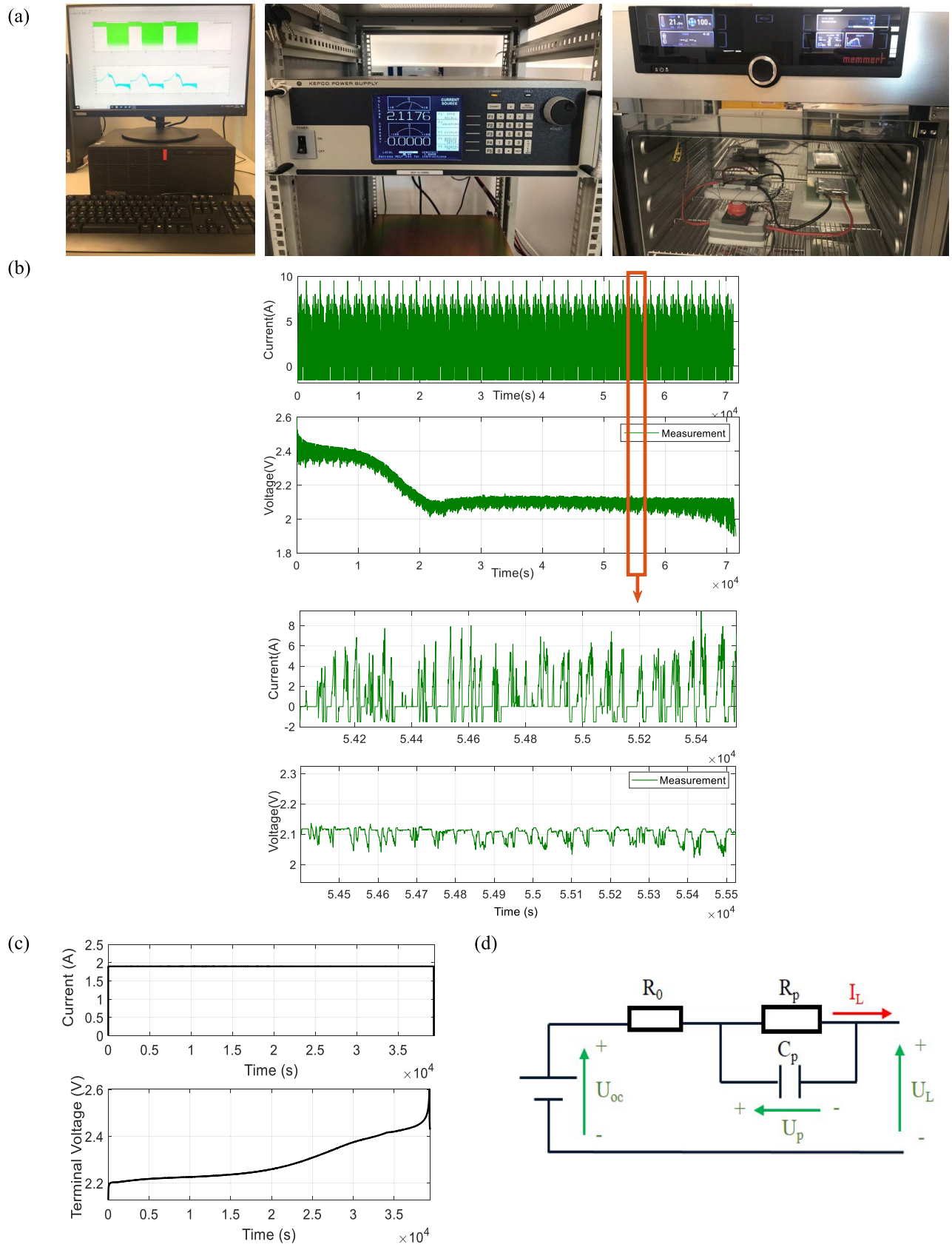


Fig. 1. Li–S cell test and modeling. (a) Test equipment including PC to control the test profile and data collection, power source/sink, and thermal chamber (from left to right). (b) Cell's current and voltage measurement in MLTB test. (c) Cell's constant current charging. (d) Thevenin model to be parameterized using the test data.

Accordingly, cell parametrization is performed at various SoC levels.

In order to generate a realistic cell current profile to simulate a standard automotive driving cycle, the power demand on the Millbrook London Transport Bus (MLTB) driving cycle [34], [35] is scaled down to be applied to a single cell. More details of the vehicle simulation and power demand calculation are presented in [36]. The proposed MLTB test results for a 19-Ah Li–S cell are shown in Fig. 1(b). As mentioned before, the current profile is repeated until the cell is depleted. To have a clearer view about this, Fig. 1(b) also presents a zoomed window including only one MLTB cycle. The test includes short charging periods in between [negative current in Fig. 1(b)] as well. This is designed to simulate regenerative braking in such an application.

Fig. 1(c) demonstrates constant-current charging profile applied in all the experiments. The charging profile is suggested by the cell manufacturer to be at constant rate of 0.1 C (i.e., 1.9 A). Investigation of the Li–S cell voltage response during charging is considered to be out of the scope of this study.

### C. Li–S Cell Modeling Approach

An ECN model is parameterized using the data obtained from the Li–S cell characterization tests. ECN modeling approach is chosen because of its effectiveness in both accuracy and computational speed [37]–[40]. A review on different battery modeling approaches is presented in [37]. In this study, an ECN model, called "Thevenin model" [41], is used as illustrated in Fig. 1(d). It consists of a voltage source $U_{\mathrm{OC}}$, representing the open circuit voltage (OCV) of the battery, and three physical components: 1) ohmic resistance ($R_{\mathrm{O}}$) that corresponds to the heating losses; 2) polarization resistance ($R_{\mathrm{P}}$); and 3) polarization capacitance ($C_{\mathrm{P}}$). According to the Thevenin model structure, dynamic behavior of the battery can be described as follows:

$$\frac{dU_p}{dt} = -\frac{1}{R_pC_p}U_p + \frac{1}{C_p}I_{\mathrm{L}} \tag{1}$$

$$U_{\mathrm{L}} = U_{\mathrm{oc}} - U_p - R_0I_{\mathrm{L}} \tag{2}$$

where $U_p$ is the voltage across the polarization capacitor, and $U_{\mathrm{L}}$ and $I_{\mathrm{L}}$ are the terminal voltage and load current, respectively.

Equation (2) can be written in frequency domain using Laplace transformation

$$s \cdot U_p(s) = -\frac{1}{R_pC_p} \cdot U_p(s) + \frac{1}{C_p}I_{\mathrm{L}}(s). \tag{3}$$

Consequently, $U_p$ can be expressed as follows:

$$U_p(s) = \frac{\frac{1}{C_p}I_{\mathrm{L}}(s)}{s + \frac{1}{R_pC_p}}. \tag{4}$$

Substituting $U_p$ from (4) into (2), terminal voltage in frequency domain is

$$U_{\mathrm{L}}(s) = U_{\mathrm{oc}} - \frac{\frac{1}{C_p}I_{\mathrm{L}}(s)}{s + \frac{1}{R_pC_p}} - R_0I_{\mathrm{L}}(s). \tag{5}$$

To transfer it from continuous-time domain to discrete-time domain, the bilinear transform

$$s = \frac{2}{T}\frac{z-1}{z+1}$$

is applied to the above equation, (6), as shown at the bottom of the page.

As a result, the terminal voltage at moment $k$ can be obtained from the current signal value at moment $k$ and the terminal voltage and current signals at previous moment $k-1$ as follows:

$$U_{\mathrm{L}}(k) = \theta_1 \cdot U_{\mathrm{L}}(k-1) + \theta_2 \cdot I_{\mathrm{L}}(k) + \theta_3 \cdot I_{\mathrm{L}}(k-1) + \theta_4 \tag{7}$$

where the parameters $\theta_1, \theta_2, \theta_3$, and $\theta_4$ are defined as follows:

$$\theta_1 = \frac{2R_pC_p - T}{T + 2R_pC_p} \tag{8}$$

$$\theta_2 = -\frac{TR_p + TR_0 + 2R_0R_pC_p}{T + 2R_pC_p} \tag{9}$$

$$\theta_3 = -\frac{TR_p + TR_0 - 2R_0R_pC_p}{T + 2R_pC_p} \tag{10}$$

$$\theta_4 = \frac{2T}{T + 2R_pC_p}U_{\mathrm{oc}}. \tag{11}$$

Equation (7) can be written in a more standard form for the later use of identification

$$U_{\mathrm{L}}(k) = \varphi^{\mathrm{T}} \cdot \theta \tag{12}$$

where $\varphi = [U_{\mathrm{L}}(k-1); I_{\mathrm{L}}(k); I_{\mathrm{L}}(k-1); 1]$ and $\theta = [\theta_1; \theta_2; \theta_3; \theta_4]$.

### D. Li–S Cell Model Parameterization Using Forgetting Factor Recursive Least Square Algorithm

Because of the application of this study in EVs, it is desirable to have a simple and quick algorithm to be applicable in real-time. Since battery parameters are changing continuously (a time-varying system), forgetting factor recursive least square (FFRLS) identification algorithm [17] is used in this study to identify parameters of the discrete model presented in (12). RLS is an identification algorithm which has been widely used in the literature [16], [17]. In RLS method, the model's error (i.e., a function of the model's parameters) is minimized using an iterative procedure [20]. Here the model has four unknown parameters to be identified: $R_0$, $R_p$, $C_p$, and $U_{\mathrm{oc}}$, which are formulated in the parameters vector $\theta$. In FFRLS algorithm, the parameters vector is updated at each iteration according to the following equation:

$$\hat{\theta}(k) = \hat{\theta}(k-1) + K(k) \cdot [U_{\mathrm{L}}(k) - \varphi^{\mathrm{T}} \cdot \hat{\theta}(k-1)] \tag{13}$$

$$\frac{U_{\mathrm{L}}(z) - U_{\mathrm{oc}}}{I_{\mathrm{L}}(z)} = \frac{-\left(TR_p + TR_0 + 2R_0R_pC_p\right) - (TR_p + TR_0 - 2R_0R_pC_p)z^{-1}}{T + 2R_pC_p + (T - 2R_pC_p)z^{-1}} \tag{6}$$

where $K$ is the correction gain obtained from

$$K(k) = P(k-1)\cdot\varphi\cdot[\gamma + \varphi^{\mathrm{T}}\cdot P(k-1)\cdot\varphi]^{-1} \quad (14)$$

$$P(k) = \frac{1}{\gamma}[I - K(k)\cdot\varphi^{\mathrm{T}}]\cdot P(k-1) \quad (15)$$

where $P$ is the covariance matrix and $\gamma$ is the forgetting factor, indicating the effect of historical data on identification.

Once $\theta_1 - \theta_4$ are estimated using the above equations, the original four physical parameters of the Thevenin model ($R_0$, $R_p$, $C_p$, and $U_{\mathrm{oc}}$) can be calculated from $\theta$ as follows:

$$R_0 = \frac{\theta_3 - \theta_2}{1+\theta_1} \quad (16)$$

$$R_p = -2\frac{\theta_1\theta_2 + \theta_3}{1-\theta_1^2} \quad (17)$$

$$C_p = \frac{T(1+\theta_1)^2}{-4(\theta_1\theta_2 + \theta_3)} \quad (18)$$

$$U_{\mathrm{oc}} = \frac{\theta_4}{1-\theta_1}. \quad (19)$$

The FFRLS identification algorithm is applied to the Li–S cell test data (presented in Section II-B) to parameterize the Thevenin model, which was illustrated in Fig. 1(d). According to the results shown in Fig. 2, the cell model's parameters are affected by both SoC and SoH. Each parameter has a unique pattern that is investigated in the following. With regard to the effect of SoC, all the parameters are showing quite similar patterns as stated in previous studies in the literature, for example, in [5]–[7] and [40]. Therefore, they are not discussed here again, because the focus of this study is on SoH. In order to investigate the effect of SoH, model identification is repeated at different age levels (i.e., shown by cycle numbers in Fig. 2). According to the results, the cell aging has different effects on each individual parameter. Parameters $U_{\mathrm{oc}}$ and $R_p$ have been affected less than the other two parameters $R_0$ and $C_p$, as the result of cell aging. For example, the OCV has not changed that much when the cell is cycled. Same conclusion is valid for the polarization resistance $R_p$. On the other hand, for the ohmic resistance, there is a clear distinction between a fresh cell and an aged cell, where an aged cell has a higher resistance. Also for the polarization capacitance, we can see some differences between a fresh cell and an aged cell. These are new outcomes of this study, which have not been discussed before in the literature. In Section III, possibility of the use of these parameters for cell SoH estimation is investigated. According to the existing identification results, the parameter $R_0$ looks more promising for that purpose.

After doing the model identification and obtaining all the four parameters, the model is validated to make sure that it generates correct outputs. For that purpose, the cell's terminal voltage, $U_{\mathrm{L}}$, is compared between the measured value and the value obtained from the identified model as illustrated in Fig. 3. The reasons of choosing the terminal voltage for the validation process are: 1) the true value of terminal voltage is available from the direct measurements during the tests and 2) the terminal voltage is considered as the output of the Thevenin model in response to a given current profile, and all the four identified parameters directly affect

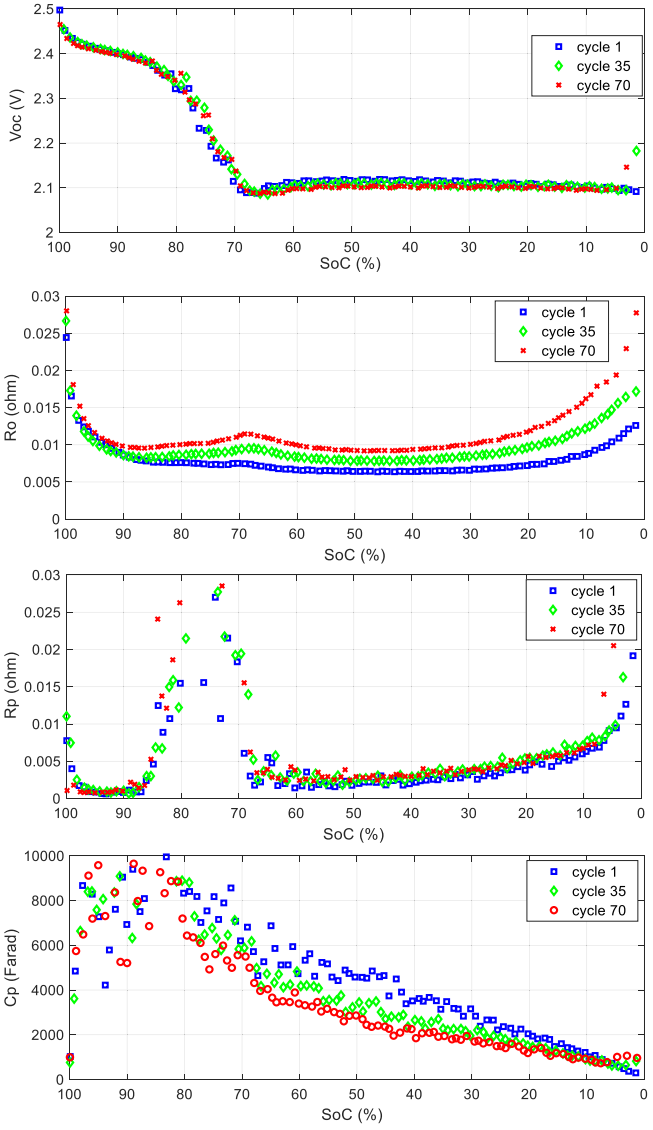


Fig. 2. Li–S cell Thevenin model's parameters versus SoC at different age levels.

the model's output. The results demonstrate that the proposed model generates very close values to the experimental measurements that proves the cell model's accuracy.

To use the results, which are presented in Fig. 2 for SoH estimation in real-time, cell's SoC is required. However, there might be an error in SoC estimation in a real application as discussed in [7] and [8]. To improve the accuracy of SoH estimation in practice, the used Ampere-hour (UAH) from fully charged state can be applied instead of SoC. It should be noted that UAH is different from coulomb-counting in terms of their calculations as explained in below. Assuming $\mathrm{SoC}_0$ as the initial SoC at time $t_0$, the cell's SoC at time $t$ is calculated as follows using coulomb-counting method:

$$\mathrm{SoC} = \mathrm{SoC}_0 - \frac{1}{C_{\mathrm{cell}}}\int_{t_0}^{t}\gamma\cdot I_{\mathrm{load}}\,d\tau \quad (20)$$

where $I_{\mathrm{load}}(t)$ is the load current (A), which is assumed positive for discharging and negative for charging, $\gamma$ is the

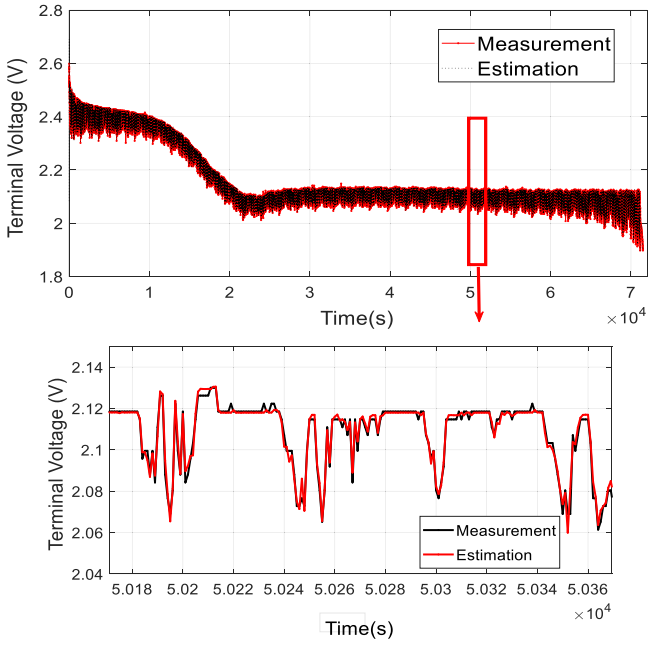


Fig. 3. Li–S cell model validation against experimental measurement.

cell's coulombic efficiency (dimensionless) and $C_{\text{cell}}$ is cell's capacity (As). In this representation, the SoC value is a number between 0 and 1 where 0 indicates fully depleted state and 1 represents fully charged state. On the other hand, UAH is defined as follows:

$$\text{UAH} = \text{UAH}_0 + \frac{1}{3600}\int_{t_0}^{t} \gamma \cdot I_{\text{load}} d\tau \tag{21}$$

where $\text{UAH}_0$ is the initial UAH value at time $t_0$, and other parameters are defined same as mentioned earlier. The constant of 3600 is added for unit conversion from (As) to (Ah). By this definition, UAH can change between 0 and maximum capacity of the cell. As we can see, in calculation of UAH, we do not use cell's capacity value ($C_{\text{cell}}$), which reduces the uncertainty of its calculation in real-time. Fig. 4 shows the same identification results but versus UAH instead of SoC. In those graphs, UAH is measured from fully charged state (i.e., $\text{UAH}_0 = 0$).

To make sure that the proposed identification method works under different working conditions, two other driving cycles are tested as well, which are the Worldwide Harmonized Light Vehicle Test Procedure (WLTP) [48] and the Urban Dynamometer Driving Schedule (UDDS) [49]. Fig. 5 shows Thevenin model's parameter identification results over three different driving cycles. According to the results, there is no remarkable difference between the identified parameters over various driving cycles, which demonstrates robustness of the proposed technique under different driving conditions.

## III. Li–S Cell SoH Estimation

In this section, a new framework is proposed for Li–S cell SoH estimation using ECN model parameterization in real-time. For this purpose, different number of identified parameters are considered and two methods are used to correlate them

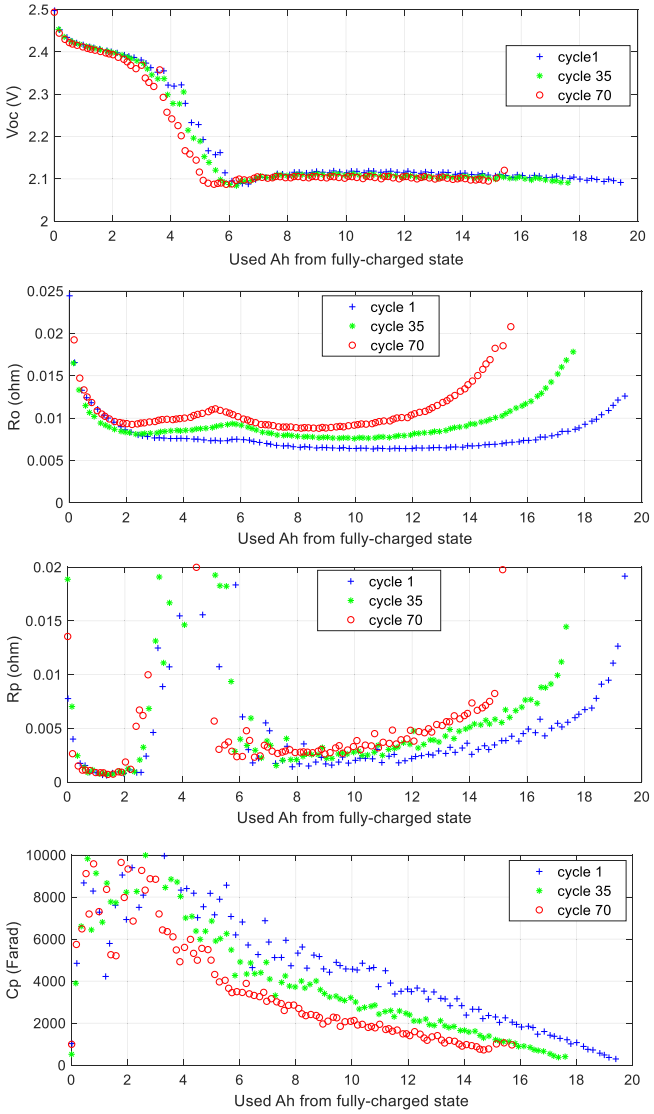


Fig. 4. Li–S cell Thevenin model's parameters versus UAH at different age levels.

to the cell's SoH: 1) first, a curve fitting technique is used when only one input parameter is available for SoH estimation and 2) second, combinations of single parameters are considered in an SVM classifier to estimate SoH using more than one parameter.

In both cases, FFRLS algorithm is used for cell model identification.

Before presenting the SoH estimation methods and their results, cell's end-of-life (EoL) is defined and capacity and power fades are analyzed according to experimental data.

### A. EoL Definition, Capacity Fade and Power Fade

In order to define a measure for battery SoH estimation, first the battery EoL should be defined. For Automotive application, there are two main definitions of battery EoL in the literature [42]. In the first definition, battery SoH is calculated by comparing the battery capacity ($Q_{\text{batt}}$) to its initial value when the battery is fresh ($Q_{\text{init}}$). In this definition,

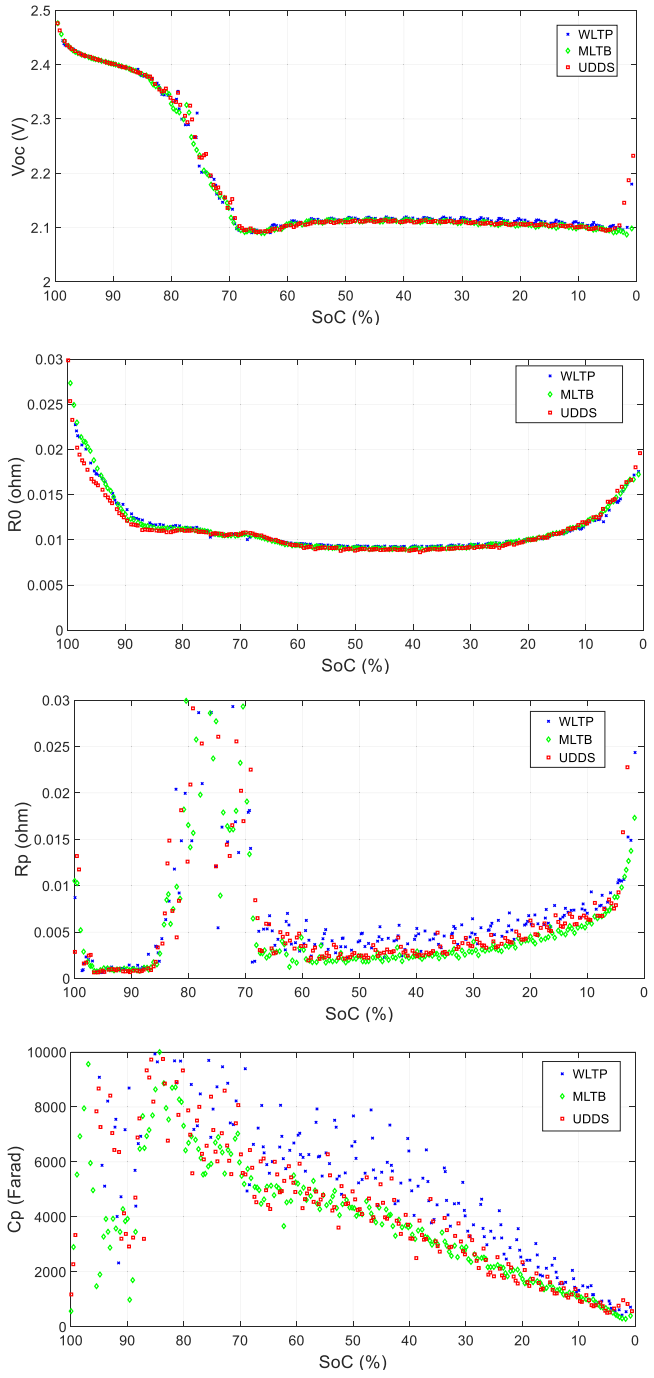


Fig. 5. Li–S cell Thevenin model's parameters identified over different driving cycles.

battery's EoL is when the capacity falls to 80% of its initial value. So, SoH can be formulated as follows:

$$\begin{aligned} \text{SoH}_Q &= 1-(Q_{\text{init}} - Q_{\text{batt}})/0.2*Q_{\text{init}} \\ 0.8Q_{\text{init}} &\le Q_{\text{batt}} \le Q_{\text{init}} \end{aligned} \tag{22}$$

where $\text{SoH}_Q$ changes between zero and one in which zero means battery EoL (i.e., $Q_{\text{batt}} = 0.8\ Q_{\text{init}}$).

In another definition of battery SoH, "power fade" is considered instead of "capacity fade." This concept is presented as battery state-of-power (SoP) in the literature too [43], [44]. The power that a battery can deliver directly depends on its ohmic resistance. The battery aging leads to an increase in the ohmic resistance in almost all types of battery. So, this parameter can be used for battery SoH estimation [47]. In one definition, battery's EoL is defined when the ohmic resistance becomes twice as its initial value as presented in the following [42]:

$$\begin{aligned} \text{SoH}_R &= 1-(R_{\text{batt}}-R_{\text{init}})/R_{\text{init}} \\ R_{\text{init}} &\le R_{\text{batt}} \le 2R_{\text{init}} \end{aligned} \tag{23}$$

where $R_{\text{init}}$ is the battery's initial ohmic resistance and $R_{\text{batt}}$ is the battery's resistance at a given time. Here $\text{SoH}_R$ changes between zero and one again showing end and beginning of battery life, respectively.

Fig. 6(a) shows capacity fade (in Ah) of the Li–S cell subject to cycling. In this study, Li–S cell's EoL is considered according to the definition stated in (20). Fig. 6(b) shows the values of $\text{SoH}_Q$ for the 19-Ah Li–S cell calculated based on capacity fade according to (20). Similarly, Fig. 6(c) illustrates the values of $\text{SoH}_R$ for the 19-Ah Li–S cell calculated based on power fade according to (21). As shown in Fig. 6(c), the minimum value of $\text{SoH}_R$ does not reach to zero for this particular type of cell because the rate of power fade (i.e., due to the increase in ohmic resistance) is slower than the rate of capacity fade. This is an interesting outcome of this article particularly for the applications where a consistent power delivery over the life of the battery is critical.

### *B. Li–S Cell SoH Estimation Using Nonlinear Curve Fitting Technique*

At a first try to design a Li–S cell SoH estimator, curve fitting technique is used to find a function that represents the relationship between SoH and one of the ECN model parameters. Referring back to the identification results presented in Section II, it was observed that the ECN model parameters change in response to cell aging. Using this fact, a SoH estimator is designed to get one of the ECN model parameters as the input and to return SoH as the output. According to the identification results, the most promising parameter to be used for this goal is the ohmic resistance (although the other parameters are also investigated in the following parts of this study). Generally, cell's ohmic resistance is a function of SoC, temperature ($T$), and SoH as follows:

$$R_o = f(\text{SoC}, T, \text{SoH}). \tag{24}$$

Here, the question is: if we know the value of $R_o$, how can we estimate the SoH? Assuming that we know the values of SoC and temperature in real-time, then the ohmic resistance can be obtained using a function like $g^*$ that returns the value of $R_o$ but at certain SoC and temperature values

$$R_o|_{\text{SoC}^*,T^*} = g^*(\text{SoH}) \tag{25}$$

where $\text{SoC}^*$ and $T^*$ are known values of SoC and temperature at a given time. If the function $g^*$ is known from laboratory experiments, then we can obtain SoH in real-time using the following formulation:

$$\text{SoH} = g^{*^{-1}}(R_o|_{\text{SoC}^*,T^*}). \tag{26}$$

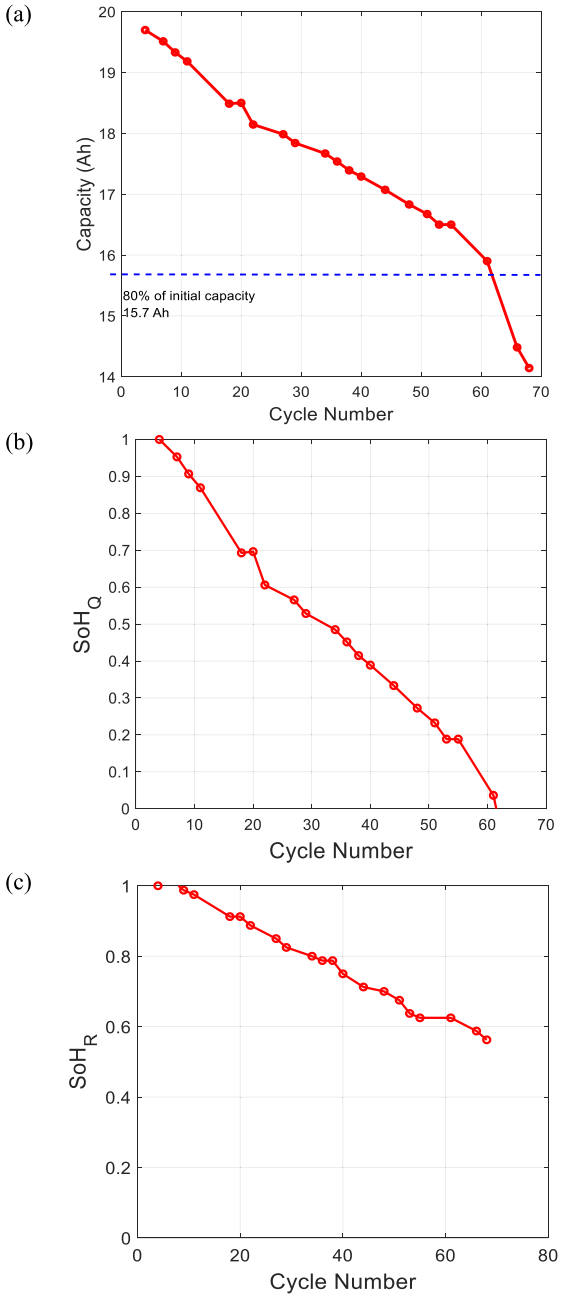


Fig. 6. (a) EoL definition based on 20% capacity fade. (b) $\mathbf{SoH_Q}$: SoH of the 19-Ah Li–S cell calculated based on capacity fade. (c) $\mathbf{SoH_R}$: SoH of the 19-Ah Li–S cell calculated based on power fade.

In this study, a constant temperature (i.e., 20 °C) is considered in all the analysis for the sake of simplicity. Considering the effect of temperature needs additional experimental tests which are time-consuming as part of the SoH design process however, the implementation phase is simple. In a real-time application, the whole range of temperature is divided into limited bands where one tuned estimator is used for each of them. The temperature can then be measured directly in real-time and the proper estimator (that is tuned at that particular temperature $T^*$) is used.

On the other hand, in order to consider the effect of SoC, a reference value (SoC*) should be agreed. In this study, various alternatives are investigated to be used as the reference

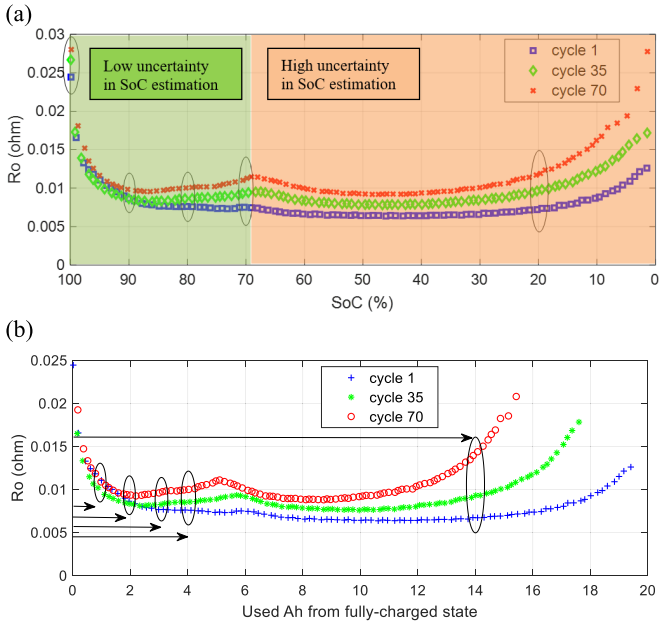


Fig. 7. Breakpoints for SoH estimation at (a) various SoC levels—there is more uncertainty in SoC value at low plateau, so, less breakpoints are selected in that area (red color) and (b) various UAH levels—the higher the UAH is, the more cumulative measurement error is expected.

SoC value including 100%, 90%, 80%, 70%, and 20%. Fig. 7(a) demonstrates those reference SoC breakpoints on the ohmic resistance curves at different cycles. As shown in Fig. 7(a), the three curves are closer to each other at some SoC values that means less sensitivity to aging. On the other hand, the distance between the curves is more at lower SoC values that means a better reflection of aging. Consequently, it is expected to see a better result when SoC* = 70% or SoC* = 20% is used compared to the other alternatives. In order to investigate this quantitatively, the curve-fitting process is repeated five times for SoC* = 100%, 90%, 80%, 70%, and 20% separately.

Another important point in Fig. 7(a) is related to the uncertainty in the value of SoC* in real-time. As mentioned before, unlike the temperature, SoC is not directly measurable and should be estimated using other techniques which is out of the framework of this study. According to the literature [6]–[8], SoC estimation of a Li–S cell is much easier at high plateau (i.e., SoC more than 75%) because of the gradient of voltage versus SoC in that plateau. That is the reason why more breakpoints are selected in that plateau as shown by green color in Fig. 7(a). In other words, although SoC* = 20% and 70% seem quite promising for SoH estimation accuracy, they are more difficult to be identified in real-time [red area in Fig. 7(a)].

Fig. 8 presents the curve fitting process for design of $\mathrm{SoH}_{\boldsymbol{Q}}$ and $\mathrm{SoH}_{\boldsymbol{R}}$ estimators using experimental data and identified values of $R_{\mathbf{o}}$ at different SoC levels. Each point in those graphs represents a single test (i.e., one cycle). Looking at the first subplot in Fig. 8, which corresponds to SoC* = 100%, it is not a good fitted curve according to the results. The reason can be found in Fig. 7(a) where there is no difference between a fresh cell and an aged cell in terms of ohmic resistance at

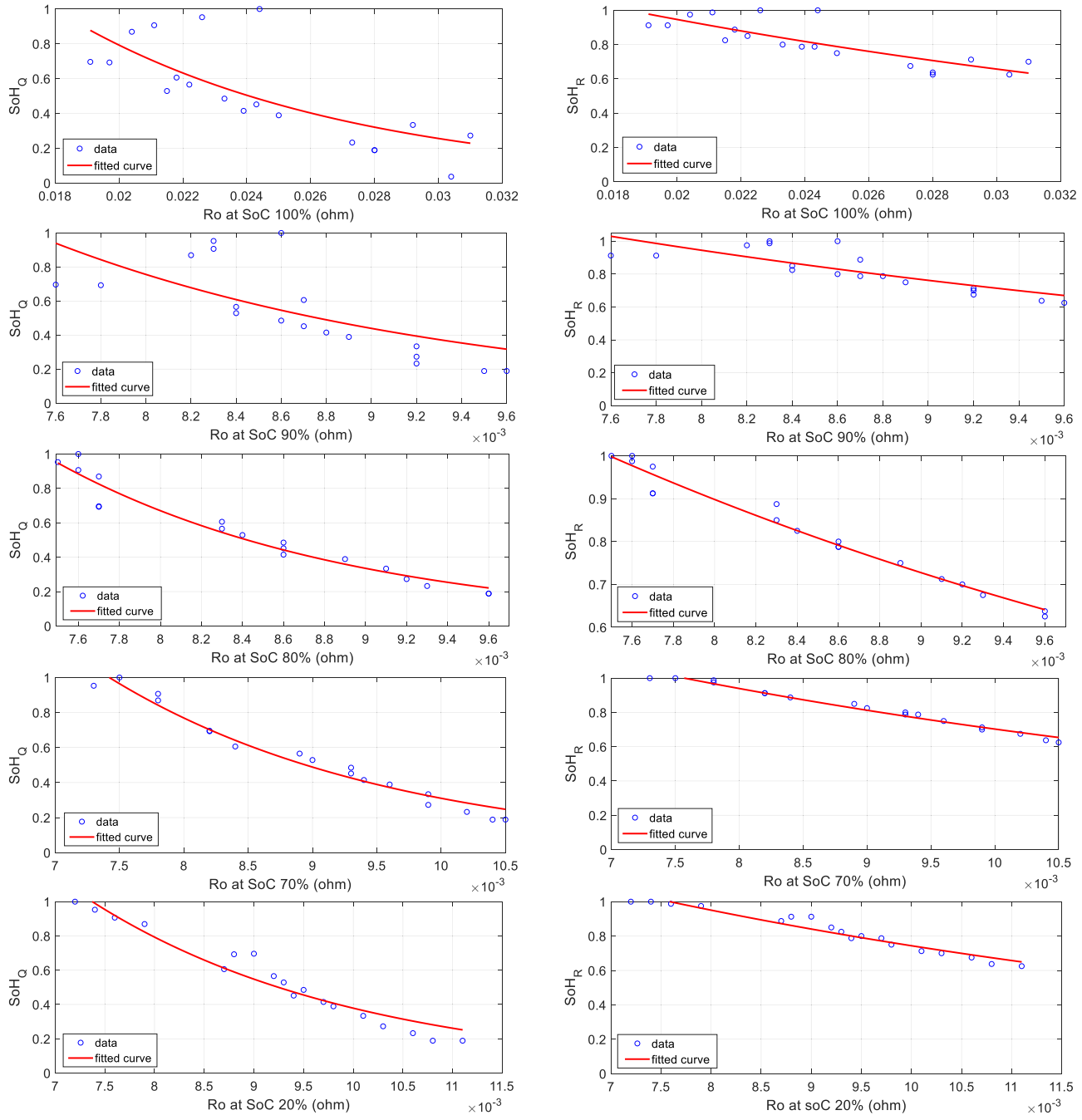


Fig. 8. Curve fitting for $\boldsymbol{SoH_Q}$ and $\boldsymbol{SoH_R}$ estimators design using training data—$\boldsymbol{R_o}$ at different SoC levels.

100% SoC. We have a very similar condition for $\text{SoC}^* = 90\%$ too, as shown in the second subplot of Fig. 8. However, when we proceed to lower SoC levels, for example 70%, there is a clear correlation between the ohmic resistance and the SoH, and consequently the fitted curve looks better.

Table II contains the root-mean-square error (RMSE) values of Li–S cell $\text{SoH}_Q$ and $\text{SoH}_R$ estimations using curve fitting technique at different SoC levels. As we expected, the best accuracy is obtained at $\text{SoC}^* = 20\%$ and 70%; however, an additional error should be added to these numbers because of the uncertainty in SoC estimation at low plateau [red area in Fig. 7(a)]. This problem is investigated in Section IV in a more systematic way by performing a sensitivity analysis on SoC estimation accuracy and its effect on SoH estimation accuracy.

Although the estimation of SoC in real-time is possible, we can simplify the SoH estimation problem by using UAH instead of SoC. UAH can be measured in real-time by integration of current over time from a reference point (i.e., fully charged state in this study). The advantage of using UAH instead of SoC is that in SoC calculation, we need to know the cell's capacity to be used in coulomb-counting method. However, the cell's capacity is subject to change due to temperature and aging. Estimation of Li–S cell SoC based on OCV

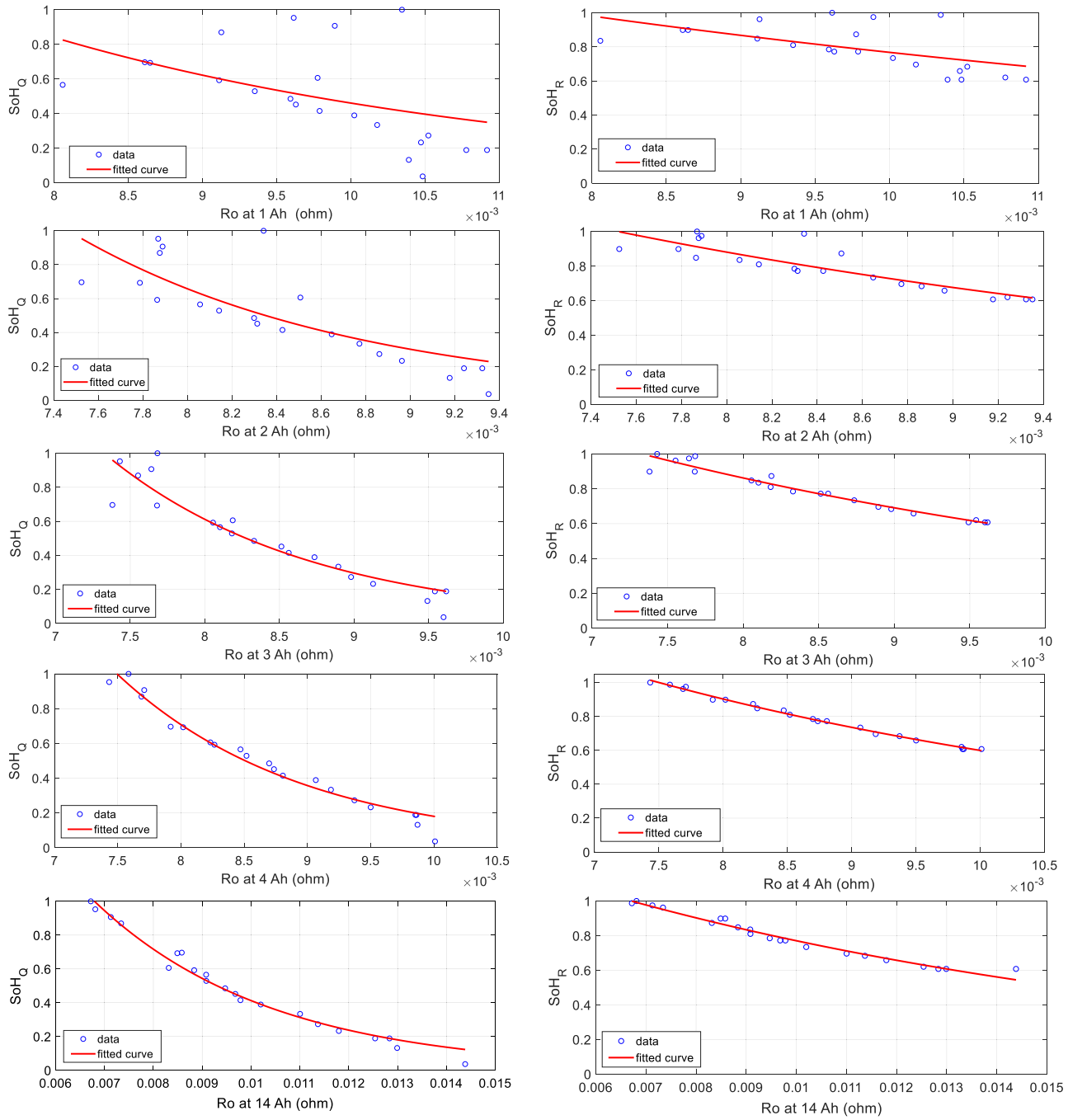


Fig. 9. Curve fitting for $\text{SoH}_Q$ and $\text{SoH}_R$ estimators design using training data—$R_o$ at different UAH levels.

TABLE II

RMSE OF $\text{SoH}_Q$ AND $\text{SoH}_R$ ESTIMATIONS USING CURVE FITTING TECHNIQUE AND $R_o$ AT DIFFERENT SOC LEVELS

| | Ro at SoC 100% | Ro at SoC 90% | Ro at SoC 80% | Ro at SoC 70% | Ro at SoC 20% |
|---|---|---|---|---|---|
| RMSE of $SoH_Q$ estimation | 21.6% | 17.3% | 7.1% | 7.1% | 8.7% |
| RMSE of $SoH_R$ estimation | 8.4% | 6.0% | 2.5% | 2.3% | 3.2% |

is not possible either as discussed in the literature [6]–[8]. The use of UAH instead of SoC provides this opportunity to get rid of solving the Li–S cell SoC estimation problem and consequently, SoH can be estimated independently.

Fig. 7(b) shows a number of alternative breakpoints for SoH estimation at various UAH levels (i.e., $\text{Ah}^* = 1$, 2, 3, 4, and 14). Any of these potential reference points can be used for SoH estimation, as long as we can detect them in

TABLE III
RMSE OF $SoH_Q$ AND $SoH_R$ ESTIMATIONS USING CURVE FITTING TECHNIQUE AND $R_o$ AT DIFFERENT UAH LEVELS

| | Ro at 1 Ah | Ro at 2 Ah | Ro at 3 Ah | Ro at 4 Ah | Ro at 14 Ah |
|---|---|---|---|---|---|
| RMSE of $SoH_Q$ estimation | 24.2 | 15.6 | 8.4 | 5.4 | 3.5 |
| RMSE of $SoH_R$ estimation | 11.0 | 5.9 | 2.6 | 1.3 | 1.6 |

TABLE IV
RMSE OF LI–S CELL $SoH_Q$ ESTIMATION USING CURVE FITTING TECHNIQUE AND DIFFERENT INPUTS AND UAH LEVELS

| | Input parameter | | | |
|---|---|---|---|---|
| | $U_{oc}$ | $R_o$ | $R_p$ | $C_p$ |
| RMSE (%) at 1 Ah | 18.62 | 24.2 | 22.16 | 26.73 |
| RMSE (%) at 2 Ah | 21.65 | 15.6 | 22.28 | 23.54 |
| RMSE (%) at 3 Ah | 25.20 | 8.4 | 12.56 | 22.38 |
| RMSE (%) at 4 Ah | 17.19 | 5.4 | 26.81 | 18.45 |
| RMSE (%) at 14 Ah | 23.31 | 3.5 | 13.84 | 13.59 |

real-time. Fig. 9 presents the curve fitting process for design of $\mathrm{SoH_Q}$ and $\mathrm{SoH_R}$ estimators using identified values of $R_o$ at different UAH levels. Again each point in those graphs represents a single test. In practice, all of the above-mentioned reference Ah* values are achievable; however, the question is which one is more accessible? A simple answer is the one which is obtained with the minimum effort, that is, $\mathrm{Ah}^* = 1$. On the other hand, Fig. 7(b) tells us that the three curves are closer/farther to each other at some Ah values that means less/more sensitivity to aging. Consequently, it is expected to see the best estimation result at $\mathrm{Ah}^* = 14$ according to Fig. 7(b) because the parameter $R_o$ changes more in response to aging. Table III contains the RMSE values of SoH estimations using curve fitting technique at different UAH levels. As it was expected, $\mathrm{Ah}^* = 14$ gives the best result; however, there is not much difference between $\mathrm{Ah}^* = 4$ and 14. Another point that should be considered in the selection process of the best Ah* is the cumulative error in Ah counting due to measurement noise in real-time. That means the higher the Ah is, the more cumulative measurement error is expected. Regarding that, $\mathrm{Ah}^* = 4$ will be more effective in real-time. So, a proper tradeoff is needed to choose between $\mathrm{Ah}^* = 4$ and 14. Overall, the preference is with $\mathrm{Ah}^* = 4$ because it is quicker to be obtained from fully charged state and with less cumulative error in Ah integration, which can potentially provide even higher level of accuracy in real-time.

Table IV contains the RMSE values of Li–S cell $\mathrm{SoH}_Q$ estimation using different inputs at different UAH levels. The results again demonstrate that the input parameter $R_o$ is the best choice to be used for Li–S cell SoH estimation in comparison to $R_p$,$C_p$, and $U_{\mathrm{oc}}$.

### C. Li–S Cell SoH Estimation Using SVM Classification Technique

In Section III-B, nonlinear curve fitting method was used to define the relationship between every single parameter of the Li–S cell model, such as $R_0$, and its SoH. An important missing point in previous section is the possibility of use of a combination of parameters instead of only one of them. It is obvious that such a solution increases the level of complexity and computational effort in comparison to the curve fitting method. However, it might be worth if the additional complexity brings a remarkable improvement in SoH estimation. In order to investigate this, all possible combinations of the four Thevenin model's parameters, $R_0$, $R_p$,$C_p$, and $U_{\mathrm{oc}}$, are considered here. In order to have a flexible estimator to serve any number of inputs, SVM classification technique is used in this section. In this new framework, FFRLS method is used for identification whereas the SVM technique is used as the SoH estimator. According to the literature, SVM method is one of the state-of-the-art techniques that is widely used for Li–ion battery state estimation in the literature. It is a quick method that is suitable for real-time applications with an acceptable level of accuracy. In [45], a good comparison between different state-of-the-art methods of battery SoH estimation is discussed which includes the SVM technique as well. The theory of the SVM as a type of a supervised machine learning method is explained in [46].

In the proposed framework, the identification results are served by the SVM classifier to estimate the range of SoH in form of a label between 1 and 10 (i.e., a cluster number). The first cluster is defined to cover the range of 0%–10% SoH, the second cluster for 10%–20% SoH, and so on. Similar to the training and validation procedure used for nonlinear curve fitting method in Section III-B, here also the data are divided into two parts: training data set and testing data set where the former is used for training the SVM and the latter is used for validation. Around 30 full tests data are used for training and another 30 tests data are used for testing. The two sets of data have been separated from the beginning to make sure that the classifiers have not seen the test data (i.e., true labels) before, to achieve a reliable outcome validation. Having ten clusters in total, around three tests data are used for each cluster in both training and testing processes.

TABLE V
RMSE OF $SoH_Q$ ESTIMATION BY SVM TECHNIQUE USING DIFFERENT INPUTS AT $Ah^* = 4$ and 14

| Input parameter(s) | RMSE (%) at 4 Ah | RMSE (%) at 14 Ah |
|---|---|---|
| $V_{oc}$ | 19.9 | 30.5 |
| $R_o$ | 4.3 | 4.1 |
| $R_p$ | 23.7 | 14.5 |
| $C_p$ | 16.4 | 11.8 |
| $U_{oc}/R_o$ | 5.6 | 8.7 |
| $U_{oc}/R_p$ | 13.1 | 13.8 |
| $U_{oc}/C_p$ | 10.2 | 11.7 |
| $R_o/R_p$ | 9.5 | 5.2 |
| $R_o/C_p$ | 10.5 | 4.5 |
| $R_p/C_p$ | 17.8 | 9.0 |
| $U_{oc}/R_o/R_p$ | 8.9 | 5.0 |
| $U_{oc}/R_o/C_p$ | 7.3 | 5.0 |
| $U_{oc}/R_p/C_p$ | 9.9 | 9.0 |
| $R_o/R_p/C_p$ | 11.7 | 5.0 |
| $U_{oc}/R_o/R_p/C_p$ | 10.1 | 4.3 |

For labeling the data, the true cluster numbers are determined according to the whole test results. After a cycling test is completed, it is split into individual cycles and the ECN parameters (i.e., the inputs of the classifier) are extracted for every single cycle. In addition, the true SoH (and consequently the true cluster label) is calculated for every single cycle by knowing the value of capacity. For the training data set, the true cluster numbers are used; however, for the testing data set, the true labels are kept aside to be used for validation only. About the other settings in SVM algorithm, it should be mentioned that the "fitcecoc" function is used in MATLAB, which fits multiclass models for SVM using the Gaussian Kernel function.

Again, the RMSE criteria are considered as a measure of accuracy of $SoH_Q$ estimations. In all RMSE calculations, the true values of SoH (that is obtained based on the true classification labels) are used after getting the estimator's output to calculate the error based on the difference between the true SoH and the estimated one. In order to calculate SoH from the SVM classifier, the middle point of each cluster is used as the output SoH value for that cluster; for example, 5% is considered when the estimated label is 1, 15% when label is 2, and so on. The estimated values are then compared with the "true SoH" values in the same way that it was performed for the curve fitting method. Table V contains the RMSE values of Li–S cell $SoH_Q$ estimation by SVM technique using different inputs at $Ah^* = 4$ and 14. For both cases of $Ah^* = 4$ and 14, the results again demonstrate that the single input parameter $R_o$ is the best choice to be used for Li–S cell SoH estimation in comparison to the other sets of input parameters. This is an interesting outcome, which also supports the results obtained in the previous section using nonlinear curve fitting technique. So, using either of those techniques, ECN model parameters $R_p$, $C_p$, and $U_{oc}$ do not help much for SoH estimation. For that reason, the nonlinear curve fitting method is preferred in comparison to SVM because both have roughly same level of accuracy but the former is simpler and easier to be implemented.

In addition to Table V, Fig. 10 also demonstrates the classification outcomes from SVM technique in the form of confusion matrices. Since the best results are obtained for the two cases of: 1) $R_o$ only and 2) all of the four parameters together, the confusion matrices are plotted for those successful cases only.

Same kind of tradeoff is valid here to choose between $Ah^* = 4$ and 14 as discussed in previous section. In Table V, the best results are 4.3% and 4.1% error values, which are obtained at $Ah^* = 4$ and 14, respectively. Overall, the preference is with $Ah^* = 4$ because it is quicker to be obtained from fully charged state and with less cumulative error in Ah integration, which can potentially provide even higher level of accuracy in real-time. That is due to an additional Ah calculation error that will be added to the estimation error. This subject is studied quantitatively in Section IV.

As a complementary analysis, the number of clusters is increased from 10 to 20, 30, and so on, in order to investigate its effect on the SoH estimation accuracy using SVM. According to the results, there is an improvement in estimation accuracy when changing the number of clusters from 10 to 20. However, this trend does not continue when using more clusters such as 30 or 50. The reason behind that outcome is related to the possibility of having empty clusters when more clusters are used. As mentioned before, around 30 full tests data are used for training the classifier. That means roughly three members in each cluster when ten clusters are considered. However, if we use 30 or more clusters, there might be some clusters without any member. Those empty clusters not only prevent any further improvement in accuracy but also might have negative effect on the training process of the classifier. Therefore, the best results are obtained when 20 clusters are considered as presented in Table VI. According to this new result, the accuracy of the estimator is around 3.3% using the best classifier.

## IV. SENSITIVITY ANALYSIS

In this section, a sensitivity analysis is performed to investigate the effect of measurement noise on the proposed SoH estimator's accuracy. Measurement noise is something inevitable especially in inexpensive applications like automotive where cost is vital. The more robust is an estimator against the noise, the least expensive devices are needed to run it in real-time. In the present case, that is Li–S cell SoH estimation, it was concluded that the proposed SoH estimator should be triggered at a certain UAH level such as $Ah^* = 4$ to get the best estimation result. Now the question is how can we determine the right time for that trigger? It was assumed that the Ah integration is calculated from fully charged state (100% charge which is detected based on maximum voltage). So, theoretically the current should be integrated over time until we reach to $Ah^* = 4$. In order to run such an algorithm in real-time, we should also consider a cumulative error that occurs in Ah integration due to the noise of the current sensor.

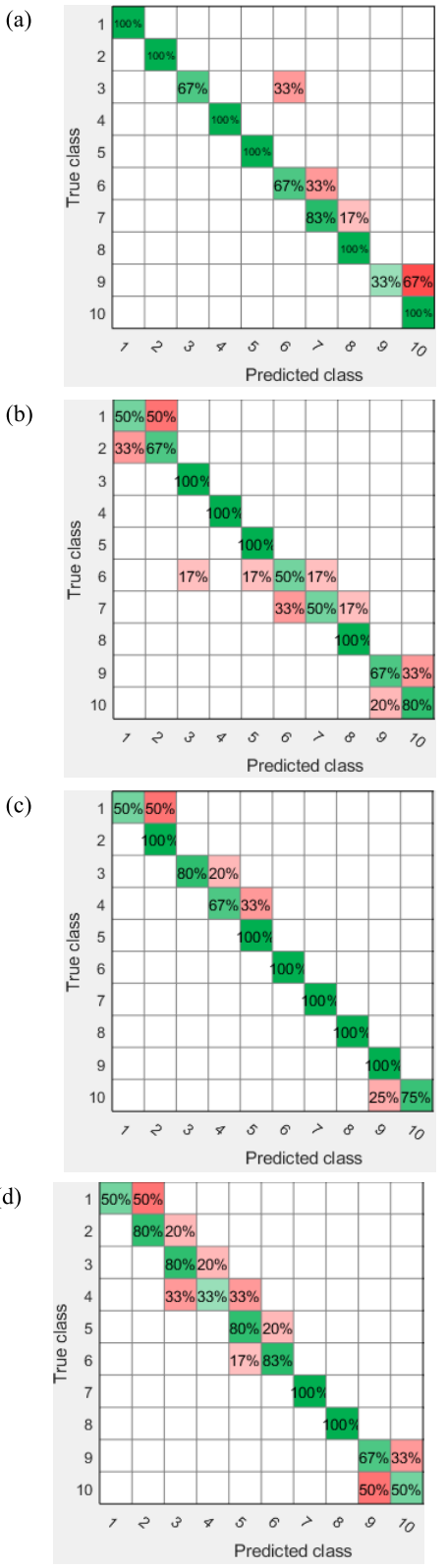


Fig. 10. Confusion matrices of SVM battery SoH classifier using different inputs. (a) $R_o$, at 4 Ah. (b) $V_{oc}$, $R_o$, $R_p$, and $C_p$ at 4 Ah. (c) $R_o$ at 14 Ah. (d) $V_{oc}$, $R_o$, $R_p$, and $C_p$, at 14 Ah.

Even a small level of noise in measurement can lead to a remarkable error over time since it has a cumulative effect. Considering that effect in our problem, the total RMSE of SoH estimation in real-time includes two elements: 1) the original

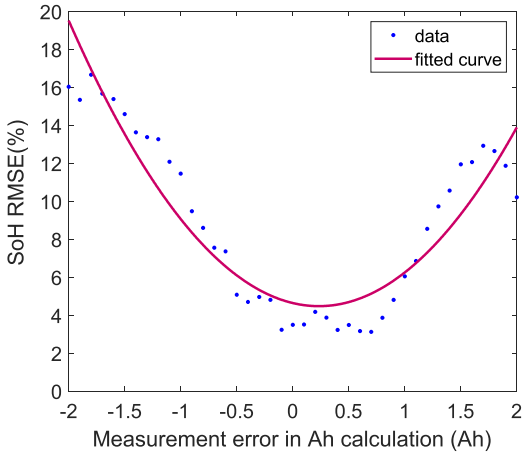


Fig. 11. Sensitivity of $\text{SoH}_Q$ estimation RMSE to UAH measurement error.

TABLE VI
RMSE OF $\text{SoH}_Q$ ESTIMATION BY SVM TECHNIQUE USING 20 CLUSTERS

| Input parameter(s) | RMSE (%) at 4 Ah | RMSE (%) at 14 Ah |
|---|---|---|
| $R_o$ | 3.30 | 3.19 |
| $U_{oc}/R_o/R_p/C_p$ | 7.91 | 4.52 |

error that comes from the estimator itself ($\text{RMSE}_{\text{estimator}}$) and 2) an additional error that comes from the measurement noise ($\text{RMSE}_{\text{noise}}$)

$$\text{RMSE}_{\text{real-time}} = \text{RMSE}_{\text{estimator}} + \text{RMSE}_{\text{noise}}. \quad (27)$$

In previous section, the value of $\text{RMSE}_{\text{estimator}}$ was obtained; however, the value of $\text{RMSE}_{\text{noise}}$ is still unknown. The effect of measurement noise is considered as an additional error in detection of the right value of $\text{Ah}^*$. For example, if $\text{Ah}^* = 4$ is desired, we might trigger the SoH estimator by mistake at $\text{Ah} = 3.9$ or $\text{Ah} = 4.1$ due to the measurement error in Ah integration over time. In order to investigate the consequence of such an error on performance of the estimator quantitatively, a sensitivity analysis is performed. Fig. 11 shows the variations of $\text{SoH}_Q$ estimation RMSE in response to different Ah measurement error values. The point zero in the horizontal axis corresponds to $\text{Ah} = 4$ that means there is no error in Ah calculation. In that case, $\text{RMSE}_{\text{real-time}}$ is just due to the estimator's error (i.e.,$\text{RMSE}_{\text{estimator}} = 3.3\%$ as stated in Table VI). Moving to the right/left from that point means to overestimate/underestimate the UAH value which causes an additional error in $\text{RMSE}_{\text{real-time}}$. According to Fig. 11, overestimation is safer than underestimation in this case. In practice, we do not expect very big errors in UAH calculation; however, an error of 0.1 or 0.2 Ah might happen in real-time for a total measurement period of 4 Ah. According to Fig. 11, an error of 0.2 Ah leads to around 1.5% additional RMSE in SoH estimation. This outcome demonstrates that the proposed estimation technique is relatively robust against the measurement noise error in UAH calculation and it can work under real working condition with RMSE around 5% ($3.3\% + 1.5\% = 4.8\%$). Although this level of accuracy is not

perfect, it is comparable with similar studies in the literature where an estimator is designed for Li–ion batteries [50], [51].

## V. Conclusion

In this study, two SoH estimators were developed for a new prototype Li–S cell using: 1) nonlinear curve fitting method when only one parameter is used and 2) SVM classification technique when a combination of parameters is used. To design and validate the estimators, a number of aging experiments were conducted on a state-of-the-art high-capacity (19 Ah) Li–S prototype pouch cell under MLTB working condition for the first time. The experimental data were then analyzed to define cell's EoL according to the two definitions in the literature: capacity fade and power fade. The results demonstrated that power fade happens in a much slower rate in comparison to the capacity fade for a Li–S cell. This is an important outcome particularly for automotive application. After that, ECN modeling technique was used to parameterize a model for the Li–S cell using FFRLS identification algorithm. The proposed idea was to perform parameter identification in real-time and then use it in a SoH estimator (e.g., a nonlinear mapping function or SVM). The advantage of the proposed technique is that it does not need the history of measurement neither the initial SoH value. According to the results, the proposed Li–S cell SoH estimation technique is quite robust against the measurement noise error in Ah calculation and it can work under conditions representative of real driving cycles with an RMSE of 3.3% when there is no noise and 4.8% in presence of noise. More research on Li–S battery technology is still going on in different areas from improving material and manufacturing to state estimation in real-time applications. Particularly for Li–S SoH estimation problem, other techniques in the literature are applicable as well, which can potentially improve the estimation accuracy.

## Acknowledgment

The authors thank OXIS Energy, U.K., for their help and support. The data used in this article are described in CORD at 10.17862/cranfield.rd.12562361; it is subject to an embargo, and will be available from April 1, 2031.

## References

[1] A. F. Hofmann, D. N. Fronczek, and W. G. Bessler, "Mechanistic modeling of polysulfide shuttle and capacity loss in lithium–sulfur batteries," *J. Power Sources*, vol. 259, pp. 300–310, Aug. 2014.

[2] G. Benveniste, H. Rallo, L. Canals Casals, A. Merino, and B. Amante, "Comparison of the state of lithium-sulphur and lithium-ion batteries applied to electromobility," *J. Environ. Manage.*, vol. 226, pp. 1–12, Nov. 2018.

[3] L. Lam and P. Bauer, "Practical capacity fading model for li-ion battery cells in electric vehicles," *IEEE Trans. Power Electron.*, vol. 28, no. 12, pp. 5910–5918, Dec. 2013.

[4] A. Fotouhi, D. J. Auger, L. O'Neill, T. Cleaver, and S. Walus, "Lithium-sulfur battery technology readiness and applications—A review," *Energies*, vol. 10, no. 12, p. 1937, 2017.

[5] K. Propp *et al.*, "Multi-temperature state-dependent equivalent circuit discharge model for lithium-sulfur batteries," *J. Power Sources*, vol. 328, pp. 289–299, Oct. 2016.

[6] A. Fotouhi, D. J. Auger, K. Propp, and S. Longo, "Electric vehicle battery parameter identification and SOC observability analysis: NiMH and Li-S case studies," *IET Power Electron.*, vol. 10, no. 11, pp. 1289–1297, 2017.

[7] A. Fotouhi, D. J. Auger, K. Propp, and S. Longo, "Lithium–sulfur battery state-of-charge observability analysis and estimation," *IEEE Trans. Power Electron.*, vol. 33, no. 7, pp. 5847–5859, Jul. 2018.

[8] K. Propp, D. J. Auger, A. Fotouhi, S. Longo, and V. Knap, "Kalman-variant estimators for state of charge in lithium-sulfur batteries," *J. Power Sources*, vol. 343, pp. 254–267, Mar. 2017.

[9] N. A. Canasa, K. Hirosea, B. Pascuccia, N. Wagnera, K. A. Friedricha, and R. Hiesgen, "Investigations of lithium–sulfur batteries using electrochemical impedance spectroscopy," *Electrochim. Acta*, vol. 97, pp. 42–51, May 2013.

[10] H.-J. Peng *et al.*, "Strongly coupled interfaces between a heterogeneous carbon host and a sulfur-containing guest for highly stable lithium-sulfur batteries: Mechanistic insight into capacity degradation," *Adv. Mater. Interfaces*, vol. 1, no. 7, Oct. 2014, Art. no. 1400227.

[11] E. Peled, M. Goor, I. Schektman, T. Mukra, Y. Shoval, and D. Golodnitsky, "The effect of binders on the performance and degradation of the Lithium/Sulfur battery assembled in the discharged state," *J. Electrochem. Soc.*, vol. 164, no. 1, pp. A5001–A5007, 2017.

[12] X. Feng, M.-K. Song, and W. C. Stolte, "Understanding the degradation mechanism of rechargeable lithium/sulfur cells: A comprehensive study of the sulfur–graphene oxide cathode after discharge–charge cycling," *Phys. Chem. Chem. Phys.*, vol. 16, no. 32, pp. 16931–16940, 2014.

[13] V. Knap, D-I. Stroe, and R. Purkayastha, "Reference performance test methodology for degradation assessment of lithium-sulfur batteries," *J. Electrochem. Soc.*, vol. 165, no. 9, pp. 1601–1609, 2018.

[14] V. Knap *et al.*, "Methodology for assessing the lithium-sulfur battery degradation for practical applications," *ECS Trans.*, vol. 77, no. 11, pp. 479–490, Jul. 2017.

[15] V. Knap, D. Auger, K. Propp, A. Fotouhi, and D.-I. Stroe, "Concurrent real-time estimation of state of health and maximum available power in lithium-sulfur batteries," *Energies*, vol. 11, no. 8, p. 2133, Aug. 2018.

[16] C. Paleologu, J. Benesty, and S. Ciochina, "A robust variable forgetting factor recursive least-squares algorithm for system identification," *IEEE Signal Process. Lett.*, vol. 15, pp. 597–600, 2008.

[17] W. K. Yung and K. F. Man, "Optimal selected forgetting factor for RLS estimation," *IFAC Proc. Volumes*, vol. 26, no. 2, pp. 331–334, Jul. 1993.

[18] Q. Wang, Z. Wang, L. Zhang, P. Liu, and Z. Zhang, "A novel consistency evaluation method for series-connected battery systems based on real-world operation data," *IEEE Trans. Transport. Electrific.*, early access, Aug. 20, 2020, doi: 10.1109/TTE.2020.3018143.

[19] X. Hu, S. E. Li, and Y. Yang, "Advanced machine learning approach for lithium-ion battery state estimation in electric vehicles," *IEEE Trans. Transport. Electrific.*, vol. 2, no. 2, pp. 140–149, Jun. 2016.

[20] H. H. Monson, "Recursive least squares," in *Statistical Digital Signal Processing and Modeling*. Hoboken, NJ, USA: Wiley, 1996, ch. 9.4, p. 541.

[21] C. Cortes and V. Vapnik, "Support-vector networks," *Mach. Learn.*, vol. 20, pp. 273–297, Sep. 1995.

[22] T. Hansen and C.-J. Wang, "Support vector based battery state of charge estimator," *J. Power Sources*, vol. 141, no. 2, pp. 351–358, Mar. 2005.

[23] X. Wu, L. Mi, W Tan, J. L. Qin, and M. N. Zhao, "State of charge (SOC) estimation of Ni-MH battery based on least square support vector machines," *Adv. Mater. Res.*, vols. 211–212, pp. 1204–1209, Mar. 2011.

[24] J. C. Álvarez Antón, P. J. García Nieto, F. J. de Cos Juez, F. Sánchez Lasheras, M. González Vega, and M. N. Roqueñí Gutiérrez, "Battery state-of-charge estimator using the SVM technique," *Appl. Math. Model.*, vol. 37, no. 9, pp. 6244–6253, May 2013.

[25] J. C. Alvarez Anton, P. J. Garcia Nieto, C. Blanco Viejo, and J. A. Vilan Vilan, "Support vector machines used to estimate the battery state of charge," *IEEE Trans. Power Electron.*, vol. 28, no. 12, pp. 5919–5926, Dec. 2013.

[26] V. Klass, M. Behm, and G. Lindbergh, "A support vector machine-based state-of-health estimation method for lithium-ion batteries under electric vehicle operation," *J. Power Sources*, vol. 270, pp. 262–272, Dec. 2014.

[27] X. Li, C. Yuan, and Z. Wang, "State of health estimation for li-ion battery via partial incremental capacity analysis based on support vector regression," *Energy*, vol. 203, Jul. 2020, Art. no. 117852.

[28] B. Saha, S. Poll, K. Goebel, and J. Christophersen, "An integrated approach to battery health monitoring using Bayesian regression and state estimation," in *Proc. IEEE Autotestcon*, Sep. 2007, pp. 646–653.

[29] J. Wei, G. Dong, and Z. Chen, "Remaining useful life prediction and state of health diagnosis for lithium-ion batteries using particle filter and support vector regression," *IEEE Trans. Ind. Electron.*, vol. 65, no. 7, pp. 5634–5643, Jul. 2018, doi: 10.1109/TIE.2017.2782224.

[30] C. She, Z. Wang, F. Sun, P. Liu, and L. Zhang, "Battery aging assessment for real-world electric buses based on incremental capacity analysis and radial basis function neural network," *IEEE Trans. Ind. Informat.*, vol. 16, no. 5, pp. 3345–3354, May 2020, doi: 10.1109/TII.2019.2951843.
[31] A. Nuhic, T. Terzimehic, T. Soczka-Guth, M. Buchholz, and K. Dietmayer, "Health diagnosis and remaining useful life prognostics of lithium-ion batteries using data-driven methods," *J. Power Sources*, vol. 239, pp. 680–688, Oct. 2013.
[32] J. Meng, L. Cai, G. Luo, D.-I. Stroe, and R. Teodorescu, "Lithium-ion battery state of health estimation with short-term current pulse test and support vector machine," *Microelectron. Rel.*, vols. 88–90, pp. 1216–1220, Sep. 2018.
[33] *Our Cell and Battery Technology Advantages*. Accessed: Sep. 1, 2020. [Online]. Available: https://oxisenergy.com/technology
[34] T. J. Barlow, S. Latham, I. S. McCrae, and P. G. Boulter, *A Reference Book of Driving Cycles for Use in the Measurement of Road Vehicle Emissions*. Wokingham, U.K.: TRL Ltd, 2009.
[35] Low Carbon Vehicle Partnership. (2018). *Testing & Accreditation–LCEB Certification*. Accessed: May 1, 2018. [Online]. Available: https://www.lowcvp.org.uk/initiatives/lceb/lceb-testing.htm
[36] V. C. Serra, A. Fotouhi, M. Soleymani, and D. J. Auger, "How suitable is lithium-sulphur battery for electric city bus application?" *Int. J. Powertrains*, vol. 9, no. 4, pp. 265–288, 2020. [Online]. Available: https://www.inderscience.com/info/ingeneral/forthcoming.php?jcode=ijpt)
[37] A. Fotouhi, D. J. Auger, K. Propp, S. Longo, and M. Wild, "A review on electric vehicle battery modelling: From lithium-ion toward lithium–sulphur," *Renew. Sustain. Energy Rev.*, vol. 56, pp. 1008–1021, Apr. 2016.
[38] H. He, R. Xiong, and J. Fan, "Evaluation of lithium-ion battery equivalent circuit models for state of charge estimation by an experimental approach," *Energies*, vol. 4, no. 4, pp. 582–598, Mar. 2011.
[39] L. Zhang, W. Fan, Z. Wang, W. Li, and D. U. Sauer, "Battery heating for lithium-ion batteries based on multi-stage alternative currents," *J. Energy Storage*, vol. 32, Dec. 2020, Art. no. 101885.
[40] A. Fotouhi, D. J. Auger, K. Propp, S. Longo, R. Purkayastha, L. O'Neill, and S. Walus, "Lithium–sulfur cell equivalent circuit network model parameterization and sensitivity analysis," *IEEE Trans. Veh. Technol.*, vol. 66, no. 9, pp. 7711–7721, Sep. 2017.
[41] Z. M. Salameh, M. A. Casacca, and W. A. Lynch, "A mathematical model for lead-acid batteries," *IEEE Trans. Energy Convers.*, vol. 7, no. 1, pp. 93–98, Mar. 1992.
[42] A. Fotouhi, K. Propp, D. J. Auger, and S. Longo, "SoC and SoH estimation on battery lifespan," in *Behaviour of Lithium-Ion Batteries in Electric Vehicles*. New York, NY, USA: Springer, 2018.
[43] A. Hoke, A. Brissette, D. Maksimovic, A. Pratt, and K. Smith, "Electric vehicle charge optimization including effects of lithium-ion battery degradation," in *Proc. IEEE Vehicle Power Propuls. Conf.*, Sep. 2011, pp. 1–8.
[44] P. Malysz, J. Ye, R. Gu, H. Yang, and A. Emadi, "Battery state-of-power peak current calculation and verification using an asymmetric parameter equivalent circuit model," *IEEE Trans. Veh. Technol.*, vol. 65, no. 6, pp. 4512–4522, Jun. 2016.
[45] C. Vidal, P. Malysz, P. Kollmeyer, and A. Emadi, "Machine learning applied to electrified vehicle battery state of charge and state of health estimation: State-of-the-art," *IEEE Access*, vol. 8, pp. 52796–52814, 2020.
[46] I. Steinwart and A. Christmann, *Support Vector Machines*. New York, NY, USA: Springer, 2008.
[47] A. Guha and A. Patra, "State of health estimation of lithium-ion batteries using capacity fade and internal resistance growth models," *IEEE Trans. Transport. Electrific.*, vol. 4, no. 1, pp. 135–146, Mar. 2018, doi: 10.1109/TTE.2017.2776558.
[48] *Worldwide Harmonized Light Vehicles Test Procedure (WLTP)–Transport–Vehicle Regulations–UNECE Wiki*. Accessed: Sep. 1, 2020. [Online]. Available: https://wiki.unece.org
[49] *EPA Urban Dynamometer Driving Schedule (UDDS)*, United States Environ. Protection Agency, Washington, DC, USA, Dec. 2015.
[50] S. Qu, Y. Kang, P. Gu, C. Zhang, and B. Duan, "A fast online state of health estimation method for lithium-ion batteries based on incremental capacity analysis," *Energies*, vol. 12, no. 17, p. 3333, Aug. 2019.
[51] C. M. Tan, P. Singh, and C. Chen, "Accurate real time on-line estimation of state-of-health and remaining useful life of Li ion batteries," *Appl. Sci.*, vol. 10, no. 21, p. 7836, 2020.

**Neda Shateri** received the M.Sc. degree in systems and control from Coventry University, Coventry, U.K., in 2018. She is currently pursuing the Ph.D. degree with the Advanced Vehicle Engineering Centre, Cranfield University, Cranfield, U.K.

Her research is focused on degradation modeling and state estimation of lithium–sulfur battery in real-world applications such as a vehicle powertrain system. She is particularly interested in investigation of the impacts of different temperature and c-rates on battery degradation. She has expertise in dynamical systems modeling and simulation, control, and optimization.

**Daniel J. Auger** (Senior Member, IEEE) was born in Rainham, U.K., in 1977. He received the M.Eng. and Ph.D. degrees from the University of Cambridge, Cambridge, U.K., in 2000 and 2005, respectively.

From 2004 to 2008, he was a Senior Engineer with BAE Systems, U.K. From 2008 to 2013, he was a Senior Consultant with MathWorks, U.K. He joined the Advanced Vehicle Engineering Centre, Cranfield University, Cranfield, U.K., in 2013, and is currently a Reader of Electrification, Automation and Control. His battery-related research interests include hybrid energy storage systems, state estimation, and electrical/thermal modeling. He also has a general interest in applications of modeling and control to vehicle systems, including driving automation and advanced driver-assistance systems (ADAS).

Dr. Auger is a former Chair of the IEEE U.K. & Ireland Control Systems Society Chapter, an IET Fellow, and a Chartered Engineer.

**Abbas Fotouhi** (Member, IEEE) received the Ph.D. degree in mechanical engineering from the Iran University of Science and Technology, Tehran, Iran, in 2011.

He was with the Centre for Artificial Intelligence (AI) and Robotics (CAIRO), University Technology Malaysia, Kuala Lumpur. In 2014, he joined Cranfield University, Cranfield, U.K., where he is currently a Lecturer (Assistant Professor) with the Advanced Vehicle Engineering Centre. He has supervised more than 40 M.Sc. and Ph.D. students so far. His expertise is dynamical systems modeling, simulation, optimization, and control. He has also extensive practical and algorithmic experience of applying AI and machine learning techniques in engineering problems. His current research includes electrified powertrain systems, batteries, and transportation system optimization.

Dr. Fotouhi is a fellow of the U.K. Higher Education Academy and the Faraday Institution in U.K.

**James Brighton** is currently a Professor of Automotive Engineering, manages the Advanced Vehicle Engineering Centre, and specializes in applied research, design, development, and postgraduate teaching in relation to advanced vehicle technology for on and off road environments together with the development of novel lightweight materials with Cranfield University, Cranfield, U.K. He has over 22-year experience relating to off road vehicle dynamics, terra-mechanics, tire and track system modeling, advanced vehicle instrumentation, lightweight material structures, and vehicle automation. He is responsible for the Cranfield Off Road Dynamics Facility, Cranfield University, which he designed and managed the delivery of together with its unique suite of research machines in collaboration with his colleagues within his previous Centre for Automotive Technology. The facility won the Henry Ford Technical Achievement Award. His team is able to offer a wide range of vehicle-related technical solutions from fundamental research through product design and prototype vehicle subsystem manufacture, supply, evaluation, and testing across a wide range of industry sectors.

Mr. Brighton is a fellow of the Institution of Agricultural Engineers (FIAgrE).